

## Many-body enhancement in a spin-chain quantum heat engine

L. A. Williamson  and Matthew J. Davis 

*ARC Centre of Excellence for Engineered Quantum Systems, School of Mathematics and Physics,  
University of Queensland, St Lucia, Queensland 4072, Australia*

 (Received 3 February 2023; revised 11 December 2023; accepted 18 December 2023; published 22 January 2024)

We show that ferromagnetic interactions can enhance the adiabatic performance of a quantum spin chain engine at low temperatures. The enhancement in work output is particularly pronounced, increasing exponentially with interaction strength. The performance enhancement occurs in the paramagnetic phase and is qualitatively explained by considering just the ground and first excited state, in which case the system exhibits bipartite entanglement. As the temperature is increased, thermal occupation of higher energy states diminishes performance. We find that these thermal fluctuations are smallest for long-range interactions, resulting in the highest efficiency. Diabatic work extraction degrades performance due to quantum friction. We identify an approximate, experimentally realisable counterdiabatic drive that can mitigate friction for weak interactions.

DOI: [10.1103/PhysRevB.109.024310](https://doi.org/10.1103/PhysRevB.109.024310)

### I. INTRODUCTION

Quantum heat engines convert heat into work utilizing some distinctly quantum effect in the reservoir or working substance [1]. Reservoirs possessing coherence [2–4], squeezing [5–11], or entanglement [12,13] have been shown to improve engine performance. Coherence in a working substance can be utilized as a resource [14–17] and can improve the power output of rapid engine cycles [18,19]. In the many-body regime, interactions in a Bose gas can enhance engine performance compared to a noninteracting gas [20–22]. Interactions in a many-body quantum system can also be tuned to change the energy of a working substance, hence providing a means to extract work [23–25].

One of the simplest quantum working substances is an ensemble of two-level systems (“spins”) [19,26–35]. Work can be extracted by tuning the level spacing  $\hbar\omega(t)$  via the control of an external field, see Fig. 1(a). Including interactions between spins opens up the possibility to explore many-body quantum effects. While considerable work has explored engines with two interacting spins [36–49], much less is known about greater numbers of spins. For nearest-neighbor interactions, a spin chain can function as both a heat engine and a refrigerator [50] with critical scaling of performance close to the critical point [51]. While moderate enhancements due to interactions have been identified in systems of two spins [42–45], a thorough investigation of whether many-body effects can improve the performance of a spin-chain quantum heat engine is lacking.

In this paper we characterize the performance of an Otto cycle with a ferromagnetic spin chain as the working substance. In addition to displaying rich many-body physics, this system may be realized in experiments with a remarkable degree of control [52–56]. We show that both short- and long-range interactions improve the adiabatic work output and efficiency in the paramagnetic phase at low temperatures  $k_B T \lesssim \hbar\omega$ . The performance enhancement is qualitatively explained by an analytic model considering just the ground and

first excited state, in which case the thermal state exhibits bipartite entanglement. For temperatures  $k_B T > \hbar\omega$ , higher energy eigenstates are occupied and interactions degrade performance. These thermal fluctuations decrease as the range of interactions is increased, and hence greater efficiency is most robust for long-range interactions. For diabatic work extraction, decreasing the engine cycle time reduces performance due to quantum friction [36,37,57]. We demonstrate an approximate, experimentally realizable counterdiabatic drive that can mitigate friction for weak interactions, and hence a performance enhancement is possible at finite power output.

This paper is organized as follows. In Sec. II we introduce the spin-chain model and the engine cycle. In Sec. III we demonstrate the performance enhancement in the adiabatic, low-temperature limit. In Sec. IV we demonstrate how increasing temperature decreases the performance enhancement. In Sec. V we show performance for finite-time work extraction, and show how a performance enhancement can be retained by using an approximate counter-diabatic drive. We conclude in Sec. VI.

### II. MODEL

A chain of  $N$  ferromagnetic interacting two-level spins is described by the Hamiltonian (hereon  $\hbar \equiv 1$ )

$$\hat{H}(\omega(t)) = -\omega(t) \sum_{i=1}^N \hat{\sigma}_z^{(i)} - g \sum_{\substack{i,j=1 \\ (j \neq i)}}^N J_{ij} \hat{\sigma}_x^{(i)} \hat{\sigma}_x^{(j)}, \quad (1)$$

with  $\hat{\sigma}_\mu^{(i)}$  ( $\mu = x, y, z$ ) the Pauli spin-1/2 matrices for spins  $i = 1, \dots, N$ . The interaction strength between spins  $i$  and  $j$  is  $gJ_{ij}$  with  $J_{ij} = 1/|i - j|^p$ ,  $g \geq 0$  the nearest-neighbor-interaction strength and  $p > 0$  determining the range of interactions. Both  $g$  and  $p$  are tuneable in experiments [53,55]. For  $N \rightarrow \infty$ , the system may be paramagnetic ( $g \lesssim \omega$ ) or ferromagnetic ( $g \gtrsim \omega$ ) with the precise cross-over  $g_c(p)$  dependent on

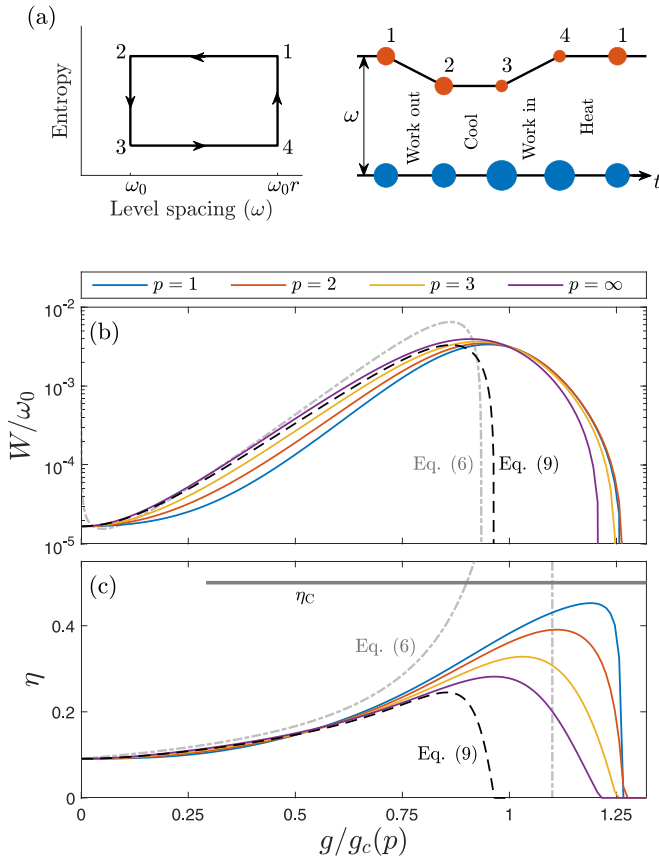


FIG. 1. (a) An Otto cycle can be realized in an ensemble of two-level spins, as described in the main text. The area of blue and red spots indicate the relative ground and excited state occupations, respectively. [(b),(c)] Engine performance for a spin chain operating adiabatically at low temperature ( $\beta_H = 10\omega_0^{-1}$ ,  $\beta_C = 2\beta_H$ ,  $N = 10$ ). Increasing  $g$  increases both (b) work output and (c) efficiency, with maximum performance at  $g \approx g_c(p)$  (results are for  $r = r_{\text{NI}}^{\text{max}}$ ). Above this, the system transitions to the ferromagnetic phase and no longer functions as an engine. The approximate  $p = \infty$  performance computed from Eq. (6) (gray dot-dashed line) and from Eq. (9) (black dashed line) are also shown. The gray horizontal line in (c) is the Carnot efficiency.

$p$  [58–64]. We denote nearest-neighbor interactions by  $p = \infty$ .

We consider an Otto engine cycle with the following steps, as shown in Fig. 1(a).

(1) We begin with a hot thermal state  $\rho_H^{\text{th}} = e^{-\beta_H \hat{H}(r\omega_0)} / Z(\beta_H, r\omega_0)$  at level spacing  $\omega = r\omega_0$ , with  $r > 1$  the “compression ratio” (in analogy with the ideal gas Otto cycle, where the compression ratio is given by the ratio of maximum and minimum gas volumes). The partition function is  $Z(\beta, \omega) = \text{Tr} e^{-\beta \hat{H}(\omega)}$  and  $\beta = (k_B T)^{-1}$  is the inverse temperature.

(1  $\rightarrow$  2) The system is then thermally isolated and work is extracted by decreasing  $\omega$  from  $r\omega_0$  to  $\omega_0$ , via the protocol  $\omega(t)/\omega_0 = f(t)$  ( $0 \leq t \leq \tau$ ). We choose  $f(t) = r + (1 - r) \sin^2(\pi t / 2\tau)$ .

(2  $\rightarrow$  3) Next, we cool the system at fixed  $\omega = \omega_0$ , leaving the system in a cold thermal state  $\rho_C^{\text{th}} = e^{-\beta_C \hat{H}(\omega_0)} / Z(\beta_C, \omega_0)$ .

(3  $\rightarrow$  4) We thermally isolate the system again and increase  $\omega$  from  $\omega_0$  back to  $r\omega_0$ , with the protocol  $\omega(t)/\omega_0 = f(\tau - t)$  ( $0 \leq t \leq \tau$ ).

(4  $\rightarrow$  1) Finally we heat the system at fixed  $\omega = r\omega_0$  back to the initial state.

The work output  $W$  and efficiency  $\eta$  of the engine cycle are

$$W = Q_H - Q_C, \quad \eta = \frac{W}{Q_H}. \quad (2)$$

Here  $Q_H = \text{Tr}[\hat{H}(r\omega_0)(\rho_H^{\text{th}} - \rho_4)]$  is the heat input from the hot reservoir and  $Q_C = -\text{Tr}[\hat{H}(\omega_0)(\rho_C^{\text{th}} - \rho_2)]$  is the heat output to the cold reservoir, with  $\rho_4$  the density matrix prior to coupling to the hot reservoir and  $\rho_2$  the density matrix prior to coupling to the cold reservoir. The density matrix at points 2 and 4 are obtained by time-evolving the von Neumann equation  $\dot{\rho}(t) = -i[H(t), \rho(t)]$  with initial conditions  $\rho_H^{\text{th}}$  and  $\rho_C^{\text{th}}$  respectively, using Runge-Kutta integration.

### III. ADIABATIC LOW-TEMPERATURE PERFORMANCE

#### A. Interactions enhance performance

We first examine the quantum adiabatic limit  $\tau \gg \omega_0^{-1}, g^{-1}$  (we set  $\tau = 100\omega_0^{-1}$ ) such that transitions between eigenstates during the work steps are suppressed [65–68]. For zero interactions and fixed  $\beta_H \omega_0 \gg 1$ , the maximum work output occurs at a compression ratio  $r_{\text{NI}}^{\text{max}} \approx 1 + (\beta_H \omega_0)^{-1}$ , which gives a small efficiency  $\eta_{\text{NI}} \approx (\beta_H \omega_0)^{-1}$  that decreases with decreasing temperature. We find that interactions in the paramagnetic phase for temperatures  $\beta_H^{-1} \ll \omega_0$ , see Figs. 1(b) and 1(c). At these low temperatures, the performance enhancement is far greater than that identified in systems of two interacting spins [42–45]. The improvement in work output is particularly pronounced, with a maximum work output  $\sim 10^2$  times larger than the noninteracting ensemble. The behavior is qualitatively similar in all cases  $p = 1, 2, 3, \infty$  after rescaling interactions by  $g_c(p)$ , which we define to be the point at which  $\partial^2 \Delta / \partial g^2|_{\omega=\omega_0}$  has a maximum (see Appendix A). Here  $\Delta$  is the energy gap to the first excited state. The improvement increases monotonically up to  $g \approx g_c(p)$ , before dropping abruptly.

We now derive an approximate analytic theory that quantitatively describes the performance enhancement for low-spin excitation and qualitatively describes the performance enhancement generally. The spin operators can be written in terms of bosonic operators via a Holstein-Primakoff transformation [69]. Expanding to quadratic order in bosonic operators gives an analytically tractable theory. To lowest order in  $g/\omega$  and for large  $N$  and  $\beta$  we obtain (see Appendix B)

$$\ln Z \approx N \mathcal{G}_p(\beta g) e^{-\beta \Delta}, \quad (3)$$

where  $N e^{-\beta \Delta}$  is the low-temperature free energy of  $N$  two-level systems with level splitting  $\Delta(\omega) = \omega - \omega_0 g / g_c$ . We have assumed a frame where the ground-state energy is zero. The factor  $\mathcal{G}_p(\beta g)$  arises from thermal fluctuations and

depends on  $p$ ,

$$\mathcal{G}_p(\beta g) \approx \begin{cases} \sqrt{\frac{1}{2\pi\beta g\zeta(p-2)}}, & p > 3, \\ \sqrt{\frac{1}{\pi\beta g(3+\ln\beta g)}}, & p = 3, \\ \frac{1}{3\beta g\zeta(2)}, & p = 2, \\ 1, & p = 1, \end{cases} \quad (4)$$

with  $\zeta(s) = \sum_{m=1}^{\infty} 1/m^s$  the Riemann zeta function.

Using Eq. (3), the system energy  $\langle E_i \rangle$  at the four points  $i = 1, 2, 3, 4$  in the cycle in Fig. 1(a) under adiabatic operation are

$$\begin{aligned} \langle E_1 \rangle &= N\Delta(r\omega_0)\mathcal{G}_p(\beta_H g)e^{-\beta_H\Delta(r\omega_0)}, \\ \langle E_2 \rangle &= N\Delta(\omega_0)\mathcal{G}_p(\beta_H g)e^{-\beta_H\Delta(r\omega_0)}, \\ \langle E_3 \rangle &= N\Delta(\omega_0)\mathcal{G}_p(\beta_C g)e^{-\beta_C\Delta(\omega_0)}, \\ \langle E_4 \rangle &= N\Delta(r\omega_0)\mathcal{G}_p(\beta_C g)e^{-\beta_C\Delta(\omega_0)}. \end{aligned} \quad (5)$$

We neglect a correction term  $\partial\mathcal{G}_p(\beta g)/\partial\beta = O(\beta^{-1}\mathcal{G}_p(\beta g))$  in Eq. (5), which is valid for low temperatures. Equation (5) gives

$$\begin{aligned} W &= N\omega_0(r-1)[\mathcal{G}_p(\beta_H g)e^{-\beta_H\Delta(r\omega_0)} - \mathcal{G}_p(\beta_C g)e^{-\beta_C\Delta(\omega_0)}], \\ \eta &= 1 - \frac{\Delta(\omega_0)}{\Delta(r\omega_0)}. \end{aligned} \quad (6)$$

For  $g < g_c(p)$ , increasing  $g$  decreases  $\Delta(\omega)$ . From examination of Eq. (6), this increases low-temperature work output as  $W \sim W_{\text{NI}}e^{\beta_H\omega_0 g/g_c}$ , consistent with the exponential increase in Fig. 1(b), and efficiency as  $\eta \sim \eta_{\text{NI}}/(1 - g/r g_c)$ . Above  $g_c$  the system transitions to the ferromagnetic state and  $\Delta$ , and therefore  $\partial^2 \ln Z / \partial\beta\partial\omega$ , changes sign. The cycle therefore no longer functions as a heat engine [50], resulting in the abrupt drop in performance above  $g_c$  in Figs. 1(b) and 1(c). The analytic result Eq. (6) for  $p = \infty$  is shown in Figs. 1(b) and 1(c).

The bosonic approximation above permits a calculation of the bipartite entanglement of the spin chain. For low temperatures, a thermal state can be approximated by  $\rho_1 \approx (|0\rangle\langle 0| + e^{-\beta\Delta}|1\rangle\langle 1|)/(1 + e^{-\beta\Delta})$ , with  $|0\rangle$  the ground state,  $|1\rangle = \sum_{i=1}^N \hat{\sigma}_+^{(i)}|0\rangle/\sqrt{N}$  the approximate first excited state (independent of  $p$ ) and  $\hat{\sigma}_+^{(i)} = \hat{\sigma}_x^{(i)} + i\hat{\sigma}_y^{(i)}$ . In Appendix C, we show that  $\rho_1$  is entangled according to the Peres-Horodecki criterion [70–72]. The performance enhancement, Eq. (6), requires access to an entangled thermal state, and so coincides with many-body quantum effects. The entanglement of  $|1\rangle$  is also directly evident from the entanglement entropy, which is  $S = \ln(N/2)$  for a partition dividing the spin chain in half, see Appendix C. In contrast, in a mean-field approximation, the interaction of spin  $i$  with the remaining spins is replaced by  $-g\Omega_i\hat{\sigma}_x^{(i)}$ . Here  $\Omega_i = 2\sum_{j\neq i} J_{ij}s_j$  is an effective transverse drive and  $s_j = \langle \hat{\sigma}_x^{(j)} \rangle_{\text{mf}}$  is a mean-field approximation for spin  $j$ . The energy gap of spin  $i$  then increases with  $g$  as  $\sqrt{\omega^2 + g^2\Omega_i^2}$  and interactions degrade performance.

In the limit of large  $N$ , a chain with nearest-neighbor interactions maps onto a system of noninteracting fermions with energies [73]

$$\mathcal{E}_\omega(\theta) = \sqrt{\omega^2 + g^2 - 2\omega g \cos\theta}. \quad (7)$$

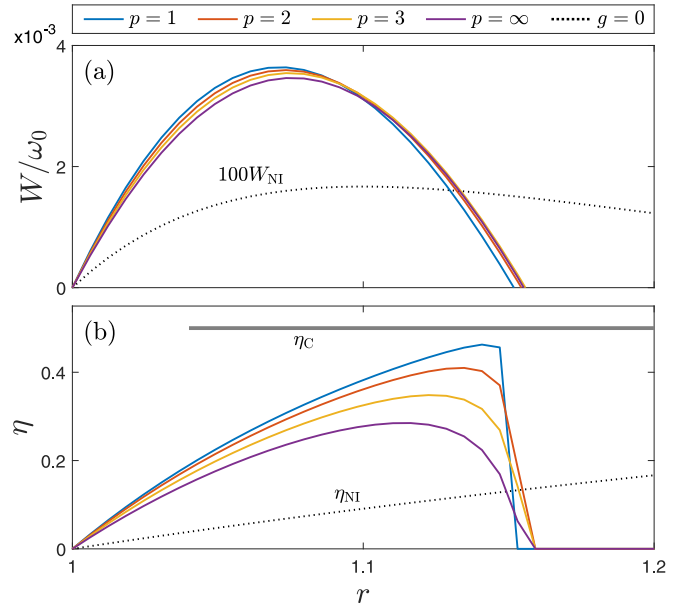


FIG. 2. Engine performance for a spin chain operating adiabatically at low temperature ( $\beta_H = 10\omega_0^{-1}$ ,  $\beta_C = 2\beta_H$ ,  $N = 10$ ). (a) Work output and (b) efficiency as a function of compression ratio for  $g = g_c(p)$ , with dotted lines indicating the noninteracting results  $W_{\text{NI}}$  and  $\eta_{\text{NI}}$  ( $W_{\text{NI}}$  is scaled by a factor of 100). The gray horizontal line in (b) is the Carnot efficiency.

For  $\beta_H^{-1} \ll \omega_0$ ,  $g$ , only the lowest-energy states are appreciably occupied. Considering only the ground state and eigenstates with singly occupied fermions gives

$$\ln Z \approx \frac{N}{\pi} \int_0^\pi e^{-\beta\mathcal{E}_\omega(\theta)} d\theta. \quad (8)$$

In the adiabatic limit, the system energies  $\langle E_i \rangle$  computed from Eq. (8) are

$$\begin{aligned} \langle E_1 \rangle &= \frac{N}{\pi} \int_0^\pi \mathcal{E}_{r\omega_0}(\theta) e^{-\beta_H\mathcal{E}_{r\omega_0}(\theta)} d\theta, \\ \langle E_2 \rangle &= \frac{N}{\pi} \int_0^\pi \mathcal{E}_{\omega_0}(\theta) e^{-\beta_H\mathcal{E}_{\omega_0}(\theta)} d\theta, \\ \langle E_3 \rangle &= \frac{N}{\pi} \int_0^\pi \mathcal{E}_{\omega_0}(\theta) e^{-\beta_C\mathcal{E}_{\omega_0}(\theta)} d\theta, \\ \langle E_4 \rangle &= \frac{N}{\pi} \int_0^\pi \mathcal{E}_{r\omega_0}(\theta) e^{-\beta_C\mathcal{E}_{\omega_0}(\theta)} d\theta. \end{aligned} \quad (9)$$

The performance computed from Eq. (9) is plotted alongside the full numerical results in Figs. 1(b) and 1(c) and agrees well with the  $p = \infty$  results for  $g < g_c$ .

### B. Effect of compression ratio

Increasing the compression ratio increases performance until  $r = r'$ , with  $r' \sim 1.1$  at  $g = g_c(p)$ . For larger compression ratio the performance abruptly drops, see Fig. 2. Unlike the noninteracting case, the peak work output and efficiency

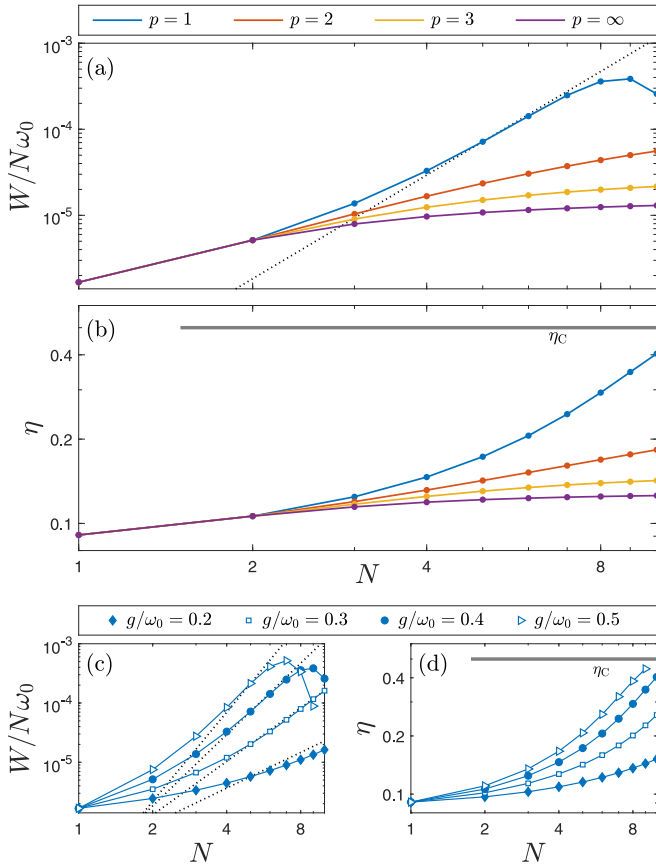


FIG. 3. The (a) work output and (b) efficiency for increasing system size for  $g = 0.4\omega_0$ , showing nonextensive scaling for  $p = 1$ . The perturbative prediction  $W \sim N^{1+\beta_H g}$  is also shown (black dotted line). [(c),(d)]  $p = 1$  performance for additional values of  $g/\omega_0$  (blue symbols) along with the perturbative predictions for  $W$  (matching black dotted lines). The gray lines in (b) and (d) are the Carnot efficiency. All results are for  $\beta_H = 10\omega_0^{-1}$ ,  $\beta_C = 2\beta_H$  and  $r = r_{\text{NI}}^{\text{max}}$ .

can both occur at a comparable compression ratio. Equation (6) describes this behavior: within this approximation, performance increases until  $1 - \Delta(\omega_0)/\Delta(r\omega_0) \sim \eta_C$ , with  $\eta_C = 1 - \beta_H/\beta_C \equiv 1 - 1/r_C$  the Carnot efficiency. Hence  $r' \approx r_C - (r_C - 1)g/g_c + O(g^2)$  decreases with increasing  $g$ . As a result, for  $g \sim g_c(p)$  we can have high efficiency at small compression ratios  $r \sim r_{\text{NI}}^{\text{max}}$ . Without interactions, the efficiency is maximum for a compression ratio  $r_C \gg r_{\text{NI}}^{\text{max}}$ .

Choosing  $\omega_0$  and  $r$  to maximise the work output in Eq. (6) gives the same efficiency as a cold two-level atom at maximum work output (ignoring corrections due to  $\mathcal{G}_p$ ). This is approximately the Curzon-Ahlborn efficiency [74]. The value of  $\omega_0$  obtained satisfies  $(1 - g/g_c)\beta_C\omega_0 \approx 1 + \eta_C^{-1} \ln r_C$ . For  $\eta_C^{-1} \ln r_C \sim 1$  and  $\beta_C\omega_0 \gg 1$ , we are close to this regime only if  $g \approx g_c$ .

### C. Finite-size scaling

The dependence of work and efficiency on chain size  $N$  is shown in Fig. 3. For  $p = \infty$  and  $p = 3$  the performance tends toward extensive scaling as  $N$  is increased. Finite-size effects are slightly more pronounced for  $p = 2$ ; however, the scaling is close to extensive. For  $p = 1$  the

performance increases nonextensively due to a dependence of  $\Delta$  on  $N$  [see inset to Fig. 6(a) in Appendix A]. Nonextensive thermodynamics is expected in systems with long-range interactions [75,76]. The critical point  $g_c$  also depends on  $N$  for  $p = 1$ . In the cold, perturbative limit (see Appendix B),  $\Delta \sim \omega - g(\gamma + \ln N)$  with  $\gamma$  the Euler-Mascheroni constant. The two-level approximation, Eq. (6), then gives  $W \sim N^{1+\beta_H g}$ . This approximation captures the dependence of work on particle number for small  $g/g_c$ , see Fig. 3(c). Increasing either  $g$  or  $N$  increases  $g/g_c$  and the perturbative approximation  $W \sim N^{1+\beta_H g}$  breaks down. Scaling  $g$  by  $g_c$  effectively Kac renormalizes the interactions, rendering the long-range system extensive [55,63,77–79].

## IV. ADIABATIC PERFORMANCE FOR INCREASING TEMPERATURE

As the temperature increases, thermal fluctuations render Eq. (6) invalid and we find that the performance enhancement relative to the noninteracting system is diminished, see Figs. 4(a) and 4(b). A performance enhancement is present as long as  $\beta_H \gtrsim 4\omega_0^{-1}$ , coinciding with the regime where only the ground and first excited state are appreciably occupied, see Fig. 4(c). The interaction strength  $g_{\text{max}}$  that gives maximum work output increases toward  $g_c(p)$  for decreasing temperature, consistent with the discussion in Sec. III B, see inset to Fig. 4(a). Curiously, we see a gradual increase in  $g_{\text{max}}$  above  $g_c(p)$  for very low temperatures. This is not accounted for by Eq. (9), and so we expect is due to finite-size effects.

The transverse Ising model gives a qualitative understanding of the diminished performance enhancement at higher temperatures. The energy levels of this model are sums of fermion energies  $\mathcal{E}_\omega(\theta_k)$ , with  $\theta_k = 2\pi k/N$  ( $k = 0, \dots, N-1$ ) [73]. Interactions diminish fermion energies with  $\cos \theta_k > g/\omega$ , with the most pronounced reduction occurring for the lowest energy fermion ( $k = 0$ ). Hence, the enhancement is largest when only the first excited state is occupied, and diminishes as more excited states are occupied [80]. The efficiency enhancement is most robust to increasing temperature for long-range interactions, see Fig. 4(b). At a given temperature  $\beta \gtrsim 4\omega_0^{-1}$ , the ratio  $\sum_{i=2}^{2^N-1} n_i/n_1$  decreases as the range of interactions increases, see Fig. 4(c). Here  $n_i = e^{-\beta E_i}/Z(\beta, \omega)$  is the thermal occupation of energy level  $i = 0, \dots, 2^N - 1$ , indexed in order of increasing energy  $E_i$ . Hence long-range interactions are most effective at suppressing fluctuations beyond the approximation (6).

For sufficiently large  $\beta_H\omega_0$ , interactions degrade performance, see Figs. 4(a) and 4(b). Expanding the dimensionless-free energy in powers of  $\beta$ , we obtain

$$\ln Z = \ln Z_\infty + \frac{N\beta^2\omega^2}{8} + \frac{\beta^2 g^2 \sum_i (\Omega'_i)^2}{8} + O(\beta^4), \quad (10)$$

with  $Z_\infty = 2^N$  the infinite temperature partition function and  $\Omega'_i = \sqrt{\frac{1}{2} \sum_{j \neq i} J_{ij}^2}$ . At order  $\beta^2$ , the free energy is indistinguishable from the mean-field free energy  $\ln \text{Tr} e^{\beta \sum_i (\omega \hat{\sigma}_i^{(0)} + g \Omega'_i \hat{\sigma}_i^{(0)})}$ , in which case interactions degrade performance. The scaling  $\ln(Z/Z_\infty) \propto \beta^2$  is clearly present for temperatures  $\beta_H \lesssim \omega_0^{-1}$ , see Fig. 4(d). For tempera-

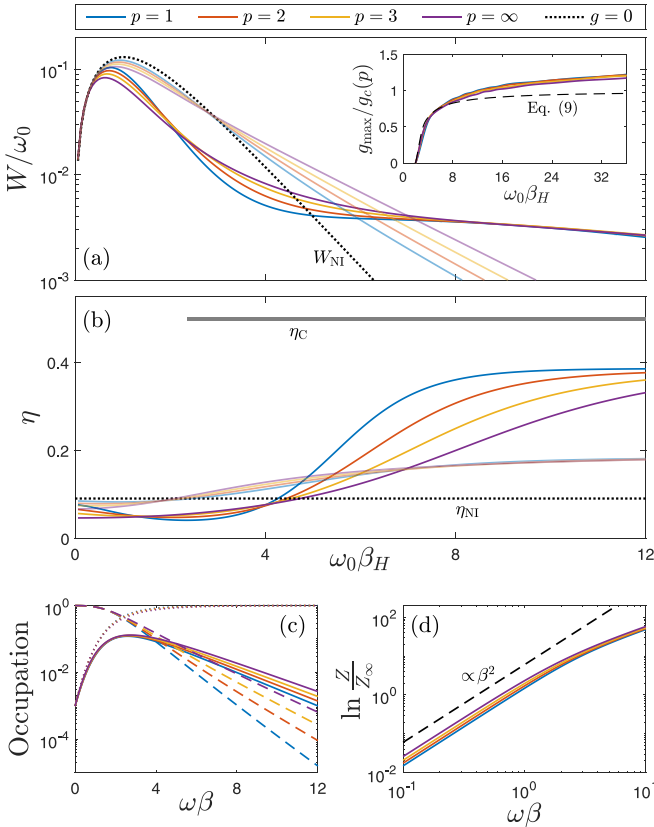


FIG. 4. Adiabatic engine performance for varying temperature. (a) Work output and (b) efficiency exceed the noninteracting values (dotted lines) for  $\beta_H \gtrsim 4\omega_0^{-1}$  [dark lines,  $g = g_c(p)$ ; light lines,  $g = 0.8g_c(p)$ ;  $r = 1.1$ ]. The gray line in (b) is the Carnot efficiency. Inset in (a) shows dependence of  $g_{\max}/g_c(p)$  on  $\beta_H$  with  $r = r_{\text{NI}}^{\max}$ ; dashed line is  $g_{\max}/g_c(p)$  computed from Eq. (9). (c) Thermal energy-level occupations  $n_0$  (dotted lines),  $n_1$  (solid lines), and  $\sum_{i=2}^{2^N-1} n_i$  (dashed lines) at  $g = g_c(p)$ . The performance enhancement occurs when occupation is predominantly in the ground and first excited state. Long-range interactions suppress occupation beyond the first excited state, resulting in the highest efficiency in (b). (d) Dimensionless free energy  $\ln Z$  at  $g = g_c(p)$  showing the  $\beta^2$  scaling (dashed line) for  $\beta \lesssim \omega^{-1}$ , coinciding with the regime of reduced performance. All results are for  $N = 10$  with  $\beta_c = 2\beta_H$ .

tures  $\beta \sim \omega_0^{-1}$ , we expect an interplay between mean-field degradation and the enhancement (6), which will govern the dependence of  $g_{\max}$  on temperatures  $\beta_H \lesssim 8\omega_0^{-1}$  [Fig. 4(a)].

## V. DIABATIC WORK EXTRACTION

For diabatic (finite-time) work extraction, interactions generally degrade engine performance due to “quantum friction” [36,37,57]. This friction arises when the interaction component of the Hamiltonian does not commute with the driving component, and hence the density matrix develops off-diagonal elements in the energy eigenbasis. The diabatic performance of a  $p = \infty$  engine with weak interactions is shown in Fig. 5(a). The peak power output occurs for a time step  $\tau \approx 4\omega_0^{-1}$  (the precise value is dependent on  $g$ ), at which

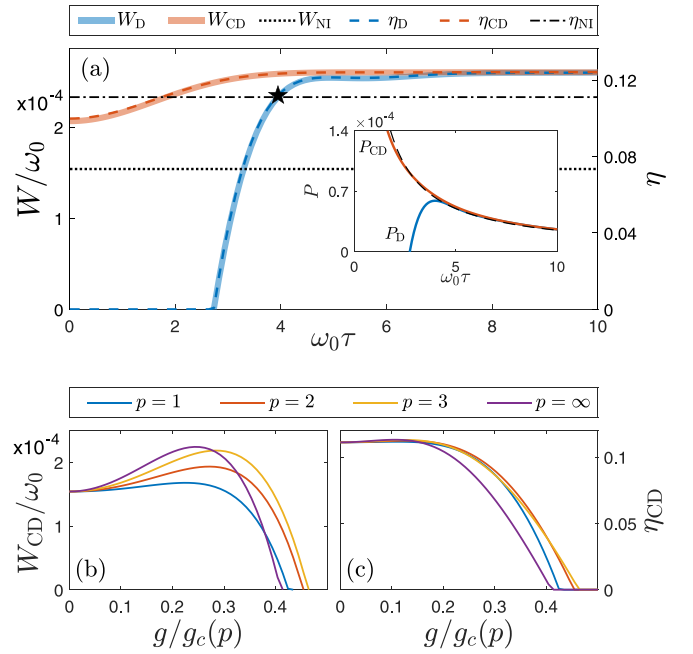


FIG. 5. (a) Diabatic work output  $W_D$  and efficiency  $\eta_D$  for  $p = \infty$  with weak interactions  $g/g_c = 0.2$ . The maximum power output  $P_D$  (see inset) occurs at  $\tau \approx 4\omega_0^{-1}$  (star), with performance rapidly declining for smaller  $\tau$ . The approximate counterdiabatic driving [Eq. (11)] results in work output ( $W_{CD}$ ) and efficiency ( $\eta_{CD}$ ) close to the adiabatic performance even for rapid engine cycles. (Inset) The power output with counterdiabatic driving  $P_{CD}$  (red line) grows  $\propto \tau^{-1}$  (black dashed line). The blue line is  $P_D$ . (b),(c) The effective-ness of Eq. (11) diminishes for larger  $g/g_c(p)$  or smaller  $p$  (results for  $\tau = \omega_0^{-1}$ ; for  $p = \infty$ , we use the exact  $\chi_{ij}$ , whereas for  $p = 1, 2, 3$ , we set  $\chi_{ij} = 1$ ). All results are for  $N = 10$  and  $r = r_{\text{NI}}^{\max}$ .

point the efficiency is close to the adiabatic efficiency. For faster cycles, the performance rapidly decreases.

In principle, quantum friction can be mitigated completely using a counterdiabatic driving field  $\hat{H}_{cd}$  [81,82]. In practice, exact counterdiabatic driving in a many-body system requires unrealistic interactions between all particles [83–89], and approximate protocols are required. A powerful approximation method is to find  $\hat{H}_{cd}$  variationally by minimizing the action  $S = \text{Tr}[G(\hat{H}_{cd})^2]$ , with  $G(\hat{H}_{cd}) = \partial \hat{H} / \partial t + i[\hat{H}_{cd}, \hat{H}]$  and  $\hat{H}_{cd}$  expanded in some truncated set of operators [90,91]. We use  $\hat{H}_{cd} = \sum_{ij(j \neq i)} C_{ij} \hat{\sigma}_x^{(i)} \hat{\sigma}_y^{(j)}$ , which is the optimal counterdiabatic drive over all one-body and two-body operators (c.f. [92]). For large  $N$  in the paramagnetic phase, we obtain (see Appendix D for details)

$$\hat{H}_{cd} = - \sum_{\substack{i,j=1 \\ (j \neq i)}}^N \frac{g\omega'(t)J_{ij}}{2\omega(t)^2} \chi_{ij}(t) \hat{\sigma}_x^{(i)} \hat{\sigma}_y^{(j)}, \quad (11)$$

with  $\chi_{ij}(t) = 1 + O(g^2/\omega^2)$  given in Appendix D. The work protocols  $f(t)$  and  $f(\tau - t)$  satisfy  $f'(0) = f'(\tau) = 0$ , and hence the net power transferred to the counterdiabatic drive field is zero. This can be shown explicitly by integrating by parts the instantaneous power  $\langle \partial(\hat{H} + \hat{H}_{cd}) / \partial t \rangle$  and noting that only the boundary term remains.

For nearest-neighbor interactions,  $\chi_{ij} = 1/(1 + g^2/\omega(t)^2)$  and Eq. (11) drastically improves the diabatic engine operation for  $g \lesssim 0.3g_c$ , see Fig. 5. For rapid cycles, the work output approaches a constant with little cost in efficiency, and hence the power output increases as  $\tau^{-1}$ , see inset to Fig. 5(a). In practice, the time scale of the thermalization steps will limit the engine to finite power [26,93]. Note  $\eta \propto W$  irrespective of counterdiabatic driving [Fig. 5(a)], hence  $Q_H$  depends only weakly on  $\tau$ .

For increasing  $g/g_c$  there is a trade-off in the performance gained from interactions and the performance lost from quantum friction, with peak performance occurring for  $g/g_c \approx 0.3$  for  $\tau = \omega_0^{-1}$ . Here, the work output from a chain with nearest-neighbor interactions is about 50% larger than the noninteracting chain and both show comparable efficiency, see Figs. 5(b) and 5(c). For  $p = 1, 2, 3$ ,  $\chi_{ij}(t)$  is difficult to engineer since the interactions must be reconfigured at different times. To simplify, we expand to lowest order in  $g/\omega$  and set  $\chi_{ij}(t) = 1$ . While this is somewhat effective at mitigating diabatic degradation for weak interactions, the performance enhancement diminishes as the range of interactions increases. Hence a chain with  $p = 1$ ,  $g/g_c \lesssim 0.3$  and  $\tau = \omega_0^{-1}$  has approximately the same performance as a noninteracting chain. Interestingly, we find that Eq. (11) is most effective for  $\beta_H \lesssim 10\omega_0^{-1}$ , with reduced performance for colder temperatures. This may be due to thermal fluctuations countering quantum friction [94].

## VI. CONCLUSIONS

We have shown that an engine of interacting spins outperforms a noninteracting engine in the paramagnetic phase for low temperatures and adiabatic operation, due to a lowering of the first excited state energy gap. The enhancement in work output is particularly pronounced, with  $W/W_{\text{NI}}$  increasing exponentially with increasing interactions. The efficiency enhancement is largest for long-range interactions, which suppress occupation of energy levels beyond the first excited state. A performance enhancement due to long-range interactions has also been identified in Kitaev chains [95,96]. For diabatic engine operation, quantum friction degrades performance. We have presented one counterdiabatic method that mitigates friction for weak interactions; however, other methods could be explored [83,89,94,97–102]. Modulating the phase and detuning of the drive profile may better isolate the two lowest energy eigenstates [103–107], limiting degradation due to thermal fluctuations and quantum friction. The low-temperature performance enhancement coincides with many-body quantum effects due to bipartite entanglement arising from the first excited state. A more thorough investigation of the entanglement properties of the thermal spin chain could reveal how entanglement changes for higher temperatures [108–111] or diabatic operation.

## ACKNOWLEDGMENTS

We thank C. Woffinden and M. Edmonds for useful comments on the manuscript. This research was supported by the Australian Research Council Centre of Excellence for Engineered Quantum Systems (EQUS, CE170100009).

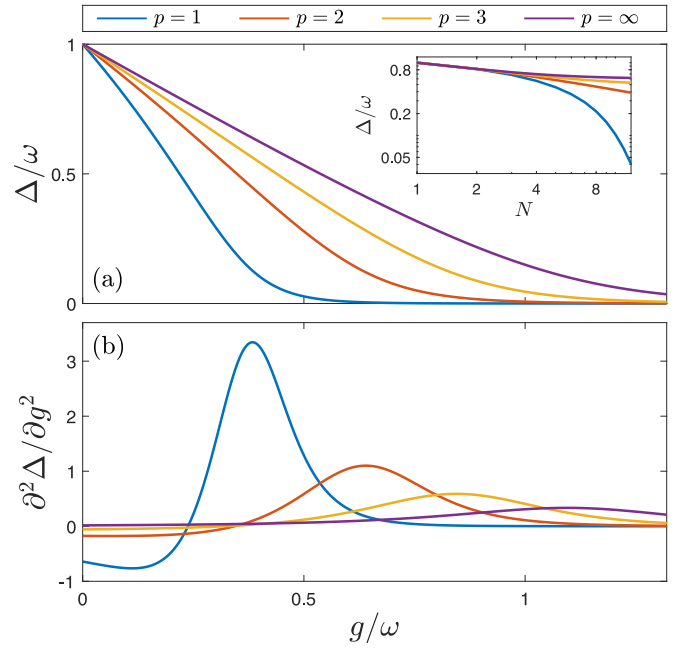


FIG. 6. (a) Energy gap  $\Delta$  between ground and first excited state for a 10-spin chain. The energy gap decreases as  $\Delta = 1 - g/g_c(p) + O(g^2)$ , where  $g_c(p)$  is the critical interaction strength separating the paramagnetic and ferromagnetic phases. In the finite-sized system, we define  $g_c(p)$  to be the point where  $\partial^2\Delta/\partial g^2$ , shown in (b), is a maximum. Inset in (a) shows the dependence of  $\Delta$  on  $N$  for  $g = 0.4\omega$ .

## APPENDIX A: DETERMINING $g_c(p)$

In this Appendix we explain how we determine the critical interaction strength  $g_c$  separating the paramagnetic and ferromagnetic phases in a finite-sized spin chain. The energy gap  $\Delta$  between the ground and first excited state is shown in Fig. 6(a). The energy gap decreases approximately linearly with increasing  $g/g_c(p)$ . In an infinite system with nearest-neighbor interactions, the exact energy gap is  $\Delta = |\omega - g|$  [73] and hence  $\partial^2\Delta/\partial g^2 = \delta(\omega - g)$ . Finite-size effects regularize the divergence of  $\partial^2\Delta/\partial g^2$ , however, we still observe a clear peak at a critical value of  $g$ , see Fig. 6(b). We define  $g_c(p)$  to be the value of  $g$  corresponding to this peak. The critical value is close to  $\omega$  for  $p = \infty$  and decreases for decreasing  $p$ . The critical value will depend on  $\omega$ . We fix  $g_c(p)$  by defining this to be the critical value at  $\omega = \omega_0$ .

## APPENDIX B: BOSONIC SPIN-WAVE APPROXIMATION

In this Appendix we derive the bosonic spin-wave approximation for the Hamiltonian (1), which leads to the approximation Eq. (6). We assume a large chain so that boundary effects can be ignored and hence we approximate the system as being translationally invariant (equivalently we can impose periodic boundary conditions). The spin operators can be converted to expressions in terms of bosonic operators via a Holstein-Primakoff transformation [69],

$$\hat{\sigma}_x^{(i)} - i\hat{\sigma}_y^{(i)} \rightarrow \left(\sqrt{1 - \hat{a}_i^\dagger \hat{a}_i}\right)\hat{a}_i, \quad \hat{\sigma}_z^{(i)} \rightarrow \frac{1}{2} - \hat{a}_i^\dagger \hat{a}_i. \quad (\text{B1})$$

In the low-excitation regime we expand the Hamiltonian (1) to quadratic order in the bosonic operators  $\hat{a}_i, \hat{a}_i^\dagger$ . This gives [69,112,113]

$$\hat{H} = -\frac{\omega N}{2} + \omega \sum_{i=1}^N \hat{a}_i^\dagger \hat{a}_i - \frac{g}{4} \sum_{\substack{i,j=1 \\ (j \neq i)}}^N J_{ij} (\hat{a}_i + \hat{a}_i^\dagger) (\hat{a}_j + \hat{a}_j^\dagger). \quad (\text{B2})$$

Fourier transforming and carrying out a Bogoliubov transformation gives [114]

$$\hat{H} = \epsilon_0 + \sum_{k=0}^{N-1} \left( \omega \text{sign}(\omega - g\tilde{J}_k) \sqrt{1 - \frac{2g}{\omega} \tilde{J}_k} \right) \hat{b}_k^\dagger \hat{b}_k, \quad (\text{B3})$$

with  $\epsilon_0$  the ground-state energy,  $\hat{b}_k$  bosonic operators for the quasiparticle modes, and

$$\tilde{J}_k = \sum_{m=1}^{N-1} \frac{\cos(2\pi km/N)}{m^p} = C_p^{N-1} \left( \frac{2\pi k}{N} \right). \quad (\text{B4})$$

Here  $C_p^N(\theta) = \sum_{m=1}^N \cos(m\theta)/m^p$  is the finite- $N$  generalized Clausen function [115]. For nearest-neighbor interactions,  $\tilde{J}_k = \cos(2\pi k/N)$  and hence  $C_\infty^N(\theta) = \cos \theta$ . From hereon we assume  $\text{sign}(\omega - g\tilde{J}_k) > 0$ .

The thermodynamic properties of the spin chain can be determined from the partition function,

$$Z = \prod_{k=0}^{N-1} \frac{1}{1 - \exp\left(-\beta\omega\sqrt{1 - \frac{2g}{\omega}\tilde{J}_k}\right)}, \quad (\text{B5})$$

with logarithm

$$\begin{aligned} \ln Z &= \sum_{k=0}^{N-1} \ln \left[ \frac{1}{1 - \exp\left(-\beta\omega\sqrt{1 - \frac{2g}{\omega}\tilde{J}_k}\right)} \right], \\ &\approx \sum_{k=0}^{N-1} \exp\left(-\beta\omega\sqrt{1 - \frac{2g}{\omega}\tilde{J}_k}\right). \end{aligned} \quad (\text{B6})$$

The latter approximation assumes low temperature. We have ignored the ground-state energy, which adds an inconsequential constant to  $\ln Z$ . To proceed analytically, we assume small  $g\tilde{J}_k/\omega$  and approximate  $\sqrt{1 - 2g\tilde{J}_k/\omega} \approx 1 - g\tilde{J}_k/\omega$ . Hence

$$\ln Z \approx e^{-\beta\omega} \sum_{k=0}^{N-1} \exp(\beta g \tilde{J}_k). \quad (\text{B7})$$

We reserve a discussion of  $p=1$  for later and for now assume  $p > 1$ . For large  $N$ ,  $C_p^{N-1}(\theta) \rightarrow C_p(\theta) = \sum_{m=1}^{\infty} \cos(m\theta)/m^p$  and we can replace the sum over  $k$  in Eq. (B7) by an integral

$$\sum_{k=0}^{N-1} \exp(\beta g \tilde{J}_k) \rightarrow \frac{N}{\pi} \int_0^\pi \exp(\beta g C_p(\theta)) d\theta \equiv N \mathcal{I}_p. \quad (\text{B8})$$

For even integers  $p$ ,

$$C_p(\theta) = -\frac{(-1)^{p/2} (2\pi)^p}{2p!} B_p \left( \frac{\theta}{2\pi} \right), \quad (\text{B9})$$

with  $B_p(x)$  the Bernoulli polynomials, which are polynomials of order  $p$ . We obtain the following results for  $p = \infty$  and  $p = 2$ ,

$$\begin{aligned} \mathcal{I}_\infty &= I_0(\beta g) \stackrel{\beta \rightarrow \infty}{\sim} \frac{e^{\beta g}}{\sqrt{2\pi\beta g}}, \\ \mathcal{I}_2 &= \frac{2e^{\beta g \pi^2/6}}{\sqrt{\beta g \pi^2}} D \left( \frac{\sqrt{\beta g \pi^2}}{2} \right) \stackrel{\beta \rightarrow \infty}{\sim} \frac{e^{\beta g \zeta(2)}}{3\beta g \zeta(2)}, \end{aligned} \quad (\text{B10})$$

where  $I_0(x)$  is the modified Bessel function,  $D(x)$  is Dawson's function (expressible in terms of the imaginary error function  $\text{erfi}(x)$  via  $D(x) = (\sqrt{\pi}/2)e^{-x^2} \text{erfi}(x)$ ), and  $\zeta(2) = \pi^2/6$ .

In general, for  $p > 3$  the integral  $\int_0^1 \exp((m\beta g C_p(2\pi x))) dx$  can be approximated at low temperatures using the method of steepest descent,

$$\mathcal{I}_p = \sqrt{\frac{1}{2\pi\beta g C_{p-2}(0)}} \exp(\beta g C_p(0)), \quad p > 3, \quad (\text{B11})$$

where  $C_p(0) = \sum_{m=1}^{\infty} m^{-p} = \zeta(p)$ . This does not work for  $p=2$  since  $C_2'(\theta)|_{\theta=0} \neq 0$ . This reflects that the spectrum is linear rather than quadratic around the lowest-energy state. Nor does it work for  $p=3$ , since  $C_3''(\theta)|_{\theta=0}$  diverges. We observe numerically that  $\exp(\beta g C_3(\theta))$  is dominated by its small  $\theta$  behavior for large  $\beta g$ . Hence for  $p=3$  we expand the Clausen function in a power series around the maximum  $\theta=0$ ,

$$C_3(\theta) \approx \zeta(3) + \frac{1}{2}\theta^2 \ln \theta - \frac{3}{4}\theta^2 + O(\theta^4). \quad (\text{B12})$$

This gives

$$\begin{aligned} \mathcal{I}_3 &\approx \frac{e^{\beta g \zeta(3)}}{\pi} \int_0^\pi \exp\left(-\frac{\beta g \theta^2}{4}(3 - 2 \ln \theta)\right) d\theta, \\ &= \frac{e^{\beta g \zeta(3)}}{\pi} \int_0^\pi \exp\left(-\frac{\beta g \theta^2}{4}(3 + \ln(\beta g) - \ln(\beta g \theta^2))\right) d\theta, \\ &= \frac{e^{\beta g \zeta(3)}}{\pi \sqrt{\beta g}} \int_0^{\pi \sqrt{\beta g}} u^{u^2/2} \exp\left(-\frac{1}{4}u^2(3 + \ln(\beta g))\right) du, \\ &\stackrel{\beta \rightarrow \infty}{\sim} \frac{e^{\beta g \zeta(3)}}{\pi \sqrt{\beta g}} \int_0^{\pi \sqrt{\beta g}} \exp\left(-\frac{1}{4}u^2(3 + \ln(\beta g))\right) du, \\ &= \frac{e^{\beta g \zeta(3)}}{\sqrt{\pi \beta g (3 + \ln \beta g)}} \text{erf}\left(\frac{\pi}{2} \sqrt{3\beta g + \beta g \ln \beta g}\right), \\ &\stackrel{\beta \rightarrow \infty}{\sim} \frac{e^{\beta g \zeta(3)}}{\sqrt{\pi \beta g (3 + \ln \beta g)}}. \end{aligned} \quad (\text{B13})$$

Hence we find a logarithmic correction  $\ln \beta g$  to the partition function for  $p=3$ , which interpolates between  $p=2$  and  $p > 3$ . The asymptotic behavior in the fourth line follows by replacing  $u^{u^2/2}$  by  $\lim_{u \rightarrow 0^+} u^{u^2/2} = 1$  due to  $\exp(-\frac{1}{4}u^2(\ln(\beta g) + 3))$  being sharply peaked around the origin for large  $\beta g$ . The validity of this approximation was confirmed numerically. Equations (B10), (B11), and (B13) give  $\ln Z = N \mathcal{G}_p(\beta g) e^{-\beta \Delta}$  with  $\Delta = \omega - g\zeta(p)$  and  $\mathcal{G}_p(\beta g)$  arising from thermal fluctuations and dependent on  $p$ .

For  $p=1$ , Eq. (B4) at  $k=0$  diverges with  $N$  as  $\tilde{J}_0 \approx \ln N + \gamma$ , with  $\gamma$  the Euler-Mascheroni constant. We separate out this term in Eq. (B7). For  $k \neq 0$ , Eq. (B4) converges and

we have

$$\sum_{m=0}^{\infty} \frac{\cos(m\theta)}{m} = C_1(\theta) = -\ln |2 \sin(\theta/2)|. \quad (\text{B14})$$

Hence

$$\ln Z \approx e^{-\beta\omega} e^{\beta g \gamma} N^{1+\beta g} + e^{-\beta\omega} \Lambda(\beta g) \quad (\text{B15})$$

with

$$\begin{aligned} \Lambda(\beta g) &= 2^{-\beta g} \sum_{k=1}^{N-1} \left( \sin \frac{\pi k}{N} \right)^{-\beta g}, \\ &= 2^{1-\beta g} \sum_{k=1}^{(N-1)/2} \left( \sin \frac{\pi k}{N} \right)^{-\beta g} \end{aligned} \quad (\text{B16})$$

arising from thermal fluctuations. We have assumed  $N$  is odd in the second line in Eq. (B16), however, even  $N$  will give the same final result below. The sum in  $\Lambda(\beta g)$  is dominated by small  $k$  terms, hence we can use the small-angle approximation  $\sin(\theta) \approx \theta$ ,

$$\begin{aligned} \Lambda(\beta g) &= 2 \left( \frac{N}{2\pi} \right)^{\beta g} \sum_{k=1}^{(N-1)/2} k^{-\beta g}, \\ &\approx 2 \left( \frac{N}{2\pi} \right)^{\beta g} \zeta(\beta g). \end{aligned} \quad (\text{B17})$$

This term is smaller than the first term in Eq. (B15) by a factor  $\sim N^{-1} (2\pi e^\gamma)^{-\beta g}$ . Hence thermal fluctuations are suppressed for low temperatures and large  $N$ , and we obtain

$$\ln Z \approx N e^{-\beta\Delta}, \quad (\text{B18})$$

with  $\Delta \approx \omega - g(\ln N + \gamma)$ . The low-temperature work output within this approximation is [see Fig. 3(a)],

$$\begin{aligned} W &\approx N \omega_0 (r-1) (e^{-\beta_H \Delta} - e^{-\beta_C \Delta}), \\ &\approx \omega_0 (r-1) e^{-\beta_H \omega_0} e^{\beta_H g \gamma} N^{1+\beta_H g}. \end{aligned} \quad (\text{B19})$$

Summarizing, to lowest order in  $g/\omega$  and for large  $N$  and  $\beta$ , we obtain the dimensionless free energies,

$$\ln Z \approx \begin{cases} \sqrt{\frac{1}{2\pi \beta g \zeta(p-2)}} e^{-\beta\Delta}, & p > 3, \\ \sqrt{\frac{1}{\pi \beta g (3+\ln \beta g)}} e^{-\beta\Delta}, & p = 3, \\ \frac{1}{3\beta g \zeta(2)} e^{-\beta\Delta}, & p = 2, \\ e^{-\beta\Delta}, & p = 1, \end{cases} \quad (\text{B20})$$

with  $\Delta(\omega) = \omega - \omega_0 g/g_c$ .

### APPENDIX C: CALCULATION OF ENTANGLEMENT

In this Appendix we calculate the low-temperature entanglement of the spin chain. Within the bosonic approximation in Appendix B, the first excited state is a state with one excitation uniformly spread across all spins,

$$|1\rangle = \frac{1}{\sqrt{N}} \sum_{i=1}^N \hat{\sigma}_+^{(i)} |0\rangle. \quad (\text{C1})$$

We consider a partition dividing the chain in half. The entanglement entropy of state  $|1\rangle$  with respect to this partition is

$$S = -\text{Tr}_R(\rho_L \ln \rho_L), \quad (\text{C2})$$

with  $\rho_L = \text{Tr}_L(|1\rangle\langle 1|)$  and  $\text{Tr}_{R(L)}$  a partial trace over states in the right(left) half of the chain. It is straightforward to show that this gives  $S = \ln(N/2)$ .

For low temperatures, we can qualitatively describe the system by the thermal state

$$\rho_1 = \frac{1}{1 + e^{-\beta\Delta}} (|0\rangle\langle 0| + e^{-\beta\Delta} |1\rangle\langle 1|), \quad (\text{C3})$$

where  $\Delta = \omega - \omega_0 g/g_c$  for small  $g/\omega$ . The Peres-Horodecki criterion states that a separable density matrix has positive partial trace [70,71]. Hence, if the density matrix does not have positive partial trace, the state is entangled (“non-PPT entanglement”). Due to the symmetry of the state, a sufficient condition for  $\rho_1$  to exhibit non-PPT entanglement is  $\text{Tr}(\hat{M} \otimes \hat{M} \rho_1) < 0$ , with  $\hat{M}$  any Hermitian operator acting on either the left ( $\hat{M} \otimes$ ) or right ( $\otimes \hat{M}$ ) partition of the chain [72]. We choose  $\hat{M} \otimes \hat{M} = \prod_{i=1}^N \hat{m}_i$  with

$$\hat{m}_i = \frac{1}{(1+\alpha)^{1/N}} [\hat{\sigma}_-^{(i)} \hat{\sigma}_+^{(i)} - \alpha \hat{\sigma}_+^{(i)} \hat{\sigma}_-^{(i)}], \quad (\text{C4})$$

with  $\alpha > 0$  a free parameter. This gives

$$\text{Tr}(\hat{M} \otimes \hat{M} \rho_1) = \frac{1 - \alpha e^{-\beta\Delta}}{(1+\alpha)(1 + e^{-\beta\Delta})}. \quad (\text{C5})$$

We can make  $\text{Tr}(\hat{M} \otimes \hat{M} \rho_1)$  arbitrarily close to  $-(1 + e^{\beta\Delta})^{-1}$  by choosing  $\alpha$  to be large ( $\alpha \gg e^{\beta\Delta}$ ). This choice of  $\hat{M}$  gives negative  $\text{Tr}(\hat{M} \otimes \hat{M} \rho_1)$  and hence the state exhibits non-PPT entanglement.

### APPENDIX D: CALCULATION OF COUNTERDIABATIC DRIVE

In this Appendix we derive the approximate counterdiabatic drive Eq. (11). We find the coefficients  $C_{ij}$  in  $\hat{H}_{\text{cd}}$  =  $\sum_{ij(j \neq i)} C_{ij} \hat{\sigma}_x^{(i)} \hat{\sigma}_y^{(j)}$  by minimizing the action

$$S = \text{Tr}(G(\hat{H}_{\text{cd}})^2), \quad (\text{D1})$$

with  $G = \frac{\partial \hat{H}}{\partial t} + i[\hat{H}_{\text{cd}}, \hat{H}]$  [90,91]. Hence we need to solve

$$\frac{\partial S}{\partial C_{ij}} = 2 \text{Tr} \left( G \frac{\partial G}{\partial C_{ij}} \right) = 0. \quad (\text{D2})$$

For notational simplicity, we set  $J_{ii} = C_{ii} = 0$ . We have

$$\begin{aligned}
 G &= -\omega'(t) \sum_p \hat{\sigma}_z^{(p)} - i\omega(t) \sum_{i,j,p} C_{ij} [\hat{\sigma}_x^{(i)} \hat{\sigma}_y^{(j)}, \hat{\sigma}_z^{(p)}] - ig \sum_{i,j,p,q} C_{ij} J_{pq} \hat{\sigma}_x^{(i)} [\hat{\sigma}_y^{(j)}, \hat{\sigma}_x^{(p)} \hat{\sigma}_x^{(q)}] \\
 &= -\omega'(t) \sum_p \hat{\sigma}_z^{(p)} + \omega(t) \sum_{i,j,p} C_{ij} (\hat{\sigma}_x^{(i)} \hat{\sigma}_x^{(j)} \delta_{pj} - \hat{\sigma}_y^{(i)} \hat{\sigma}_y^{(j)} \delta_{pi}) - g \sum_{i,j,p,q} C_{ij} J_{pq} \hat{\sigma}_x^{(i)} (\hat{\sigma}_z^{(p)} \hat{\sigma}_x^{(q)} \delta_{jp} + \hat{\sigma}_x^{(p)} \hat{\sigma}_z^{(q)} \delta_{jq}) \\
 &= -\omega'(t) \sum_p \hat{\sigma}_z^{(p)} + \omega(t) \sum_{i,j} C_{ij} (\hat{\sigma}_x^{(i)} \hat{\sigma}_x^{(j)} - \hat{\sigma}_y^{(i)} \hat{\sigma}_y^{(j)}) - 2g \sum_{i,p,q} J_{pq} C_{ip} \hat{\sigma}_x^{(i)} \hat{\sigma}_x^{(q)} \hat{\sigma}_z^{(p)}.
 \end{aligned} \tag{D3}$$

Hence

$$\frac{\partial G}{\partial C_{mn}} = \omega(t) (\hat{\sigma}_x^{(m)} \hat{\sigma}_x^{(n)} - \hat{\sigma}_y^{(m)} \hat{\sigma}_y^{(n)}) - 2g \sum_{\ell} J_{n\ell} \hat{\sigma}_x^{(m)} \hat{\sigma}_x^{(\ell)} \hat{\sigma}_z^{(n)}. \tag{D4}$$

We now want to calculate the trace of  $G\partial G/\partial C_{mn}$  ( $m \neq n$ ). The three terms in  $G$  and the two terms in  $\partial G/\partial C_{mn}$  gives a total of six terms. Three of these are zero, since the trace of terms with an odd number of spin-1/2 operators is zero. The three remaining terms are

$$\text{Tr} \left[ 2g\omega'(t) \sum_p \hat{\sigma}_z^{(p)} \sum_{\ell} J_{n\ell} \hat{\sigma}_x^{(m)} \hat{\sigma}_x^{(\ell)} \hat{\sigma}_z^{(n)} \right] = 2^N \frac{g\omega'(t) J_{mn}}{8}. \tag{D5}$$

$$\text{Tr} \left[ \omega(t)^2 \sum_{p,q} C_{pq} (\hat{\sigma}_x^{(p)} \hat{\sigma}_x^{(q)} - \hat{\sigma}_y^{(p)} \hat{\sigma}_y^{(q)}) (\hat{\sigma}_x^{(m)} \hat{\sigma}_x^{(n)} - \hat{\sigma}_y^{(m)} \hat{\sigma}_y^{(n)}) \right] = 2^N \frac{\omega(t)^2 C_{mn}}{4}. \tag{D6}$$

$$\text{Tr} \left[ 4g^2 \sum_{p,q,r} J_{pq} C_{pr} \hat{\sigma}_x^{(r)} \hat{\sigma}_x^{(q)} \hat{\sigma}_z^{(p)} \sum_{\ell} J_{n\ell} \hat{\sigma}_x^{(m)} \hat{\sigma}_x^{(\ell)} \hat{\sigma}_z^{(n)} \right] = 2^N \frac{g^2 (J_{mn}(JC)_{nn} + \frac{1}{2}(J^2)_{nn} C_{mn} - J_{mn}^2 C_{mn})}{8}. \tag{D7}$$

Combining terms gives the coupled linear equations that determine  $C_{mn}$ ,

$$g\omega'(t) J_{mn} + 2\omega(t)^2 C_{mn} + g^2 (J_{mn}(JC)_{nn} + \frac{1}{2}(J^2)_{nn} C_{mn} - J_{mn}^2 C_{mn}) = 0. \tag{D8}$$

This gives

$$C_{mn} = -\frac{g\omega'(t) J_{mn} + g^2 J_{mn}(JC)_{nn}}{2\omega(t)^2 + g^2 [\frac{1}{2}(J^2)_{nn} - J_{mn}^2]}. \tag{D9}$$

Multiplying both sides by  $g^2 J_{mn}$  and summing over  $m$  gives

$$g^2 (JC)_{nn} = -(g\omega'(t) + g^2 (JC)_{nn}) \lambda_n, \tag{D10}$$

with

$$\lambda_n = \sum_m \frac{g^2 J_{mn}^2}{2\omega(t)^2 + g^2 [\frac{1}{2}(J^2)_{nn} - J_{mn}^2]}. \tag{D11}$$

Equation (D10) can be rearranged to give

$$g^2 (JC)_{nn} = -\frac{g\omega'(t) \lambda_n}{1 + \lambda_n}. \tag{D12}$$

Substituting this into Eq. (D9) gives

$$C_{mn} = -\frac{g\omega'(t) (\frac{1}{1+\lambda_n}) J_{mn}}{2\omega(t)^2 + g^2 [\frac{1}{2}(J^2)_{nn} - J_{mn}^2]}. \tag{D13}$$

For an infinite chain with  $J_{mn} = 1/|m-n|^p$ ,  $(J^2)_{nn}/2 = \zeta(2p)$ , and  $\lambda_n = \lambda$  is independent of  $n$ . For nearest-neighbor interactions,  $\lambda = g^2/\omega(t)^2$ , and

$$C_{mn} = -\frac{g\omega'(t)}{2(\omega(t)^2 + g^2)} \delta_{n,m+1}. \tag{D14}$$

Using Mathematica, we find that  $\lambda$  can be evaluated analytically for selected values of  $p$ . For example, for  $p = 1$ ,  $\lambda = 1 - x \cot x$  with  $x = \pi g/\sqrt{2\omega(t)^2 + \zeta(2)g^2}$ .

- [1] J. Millen and A. Xuereb, Perspective on quantum thermodynamics, *New J. Phys.* **18**, 011002 (2016).
- [2] M. O. Scully, M. S. Zubairy, G. S. Agarwal, and H. Walther, Extracting work from a single heat bath via vanishing quantum coherence, *Science* **299**, 862 (2003).
- [3] A. Ü. C. Hardal and Ö. E. Müstecaplıoğlu, Superradiant quantum heat engine, *Sci. Rep.* **5**, 12953 (2015).
- [4] K. Hammam, H. Leitch, Y. Hassouni, and G. De Chiara, Exploiting coherence for quantum thermodynamic advantage, *New J. Phys.* **24**, 113053 (2022).
- [5] X. L. Huang, T. Wang, and X. X. Yi, Effects of reservoir squeezing on quantum systems and work extraction, *Phys. Rev. E* **86**, 051105 (2012).
- [6] J. Roßnagel, O. Abah, F. Schmidt-Kaler, K. Singer, and E. Lutz, Nanoscale heat engine beyond the Carnot limit, *Phys. Rev. Lett.* **112**, 030602 (2014).
- [7] G. Manzano, F. Galve, R. Zambrini, and J. M. R. Parrondo, Entropy production and thermodynamic power of the squeezed thermal reservoir, *Phys. Rev. E* **93**, 052120 (2016).
- [8] W. Niedenzu, D. Gelbwaser-Klimovsky, A. G. Kofman, and G. Kurizki, On the operation of machines powered by quantum non-thermal baths, *New J. Phys.* **18**, 083012 (2016).
- [9] J. Klaers, S. Faelt, A. Imamoglu, and E. Togan, Squeezed thermal reservoirs as a resource for a nanomechanical engine beyond the Carnot limit, *Phys. Rev. X* **7**, 031044 (2017).
- [10] B. K. Agarwalla, J.-H. Jiang, and D. Segal, Quantum efficiency bound for continuous heat engines coupled to non-canonical reservoirs, *Phys. Rev. B* **96**, 104304 (2017).
- [11] W. Niedenzu, V. Mukherjee, A. Ghosh, A. G. Kofman, and G. Kurizki, Quantum engine efficiency bound beyond the second law of thermodynamics, *Nat. Commun.* **9**, 165 (2018).
- [12] R. Dillenschneider and E. Lutz, Energetics of quantum correlations, *Europhys. Lett.* **88**, 50003 (2009).
- [13] O. Abah and E. Lutz, Efficiency of heat engines coupled to nonequilibrium reservoirs, *Europhys. Lett.* **106**, 20001 (2014).
- [14] P. Kammerlander and J. Anders, Coherence and measurement in quantum thermodynamics, *Sci. Rep.* **6**, 22174 (2016).
- [15] K. Korzekwa, M. Lostaglio, J. Oppenheim, and D. Jennings, The extraction of work from quantum coherence, *New J. Phys.* **18**, 023045 (2016).
- [16] R. Uzdin, Coherence-induced reversibility and collective operation of quantum heat machines via coherence recycling, *Phys. Rev. Applied* **6**, 024004 (2016).
- [17] H. Tajima and K. Funo, Superconducting-like heat current: Effective cancellation of current-dissipation trade-off by quantum coherence, *Phys. Rev. Lett.* **127**, 190604 (2021).
- [18] R. Uzdin, A. Levy, and R. Kosloff, Equivalence of quantum heat machines, and quantum-thermodynamic signatures, *Phys. Rev. X* **5**, 031044 (2015).
- [19] J. Klatzow, J. N. Becker, P. M. Ledingham, C. Weinzettl, K. T. Kaczmarek, D. J. Saunders, J. Nunn, I. A. Walmsley, R. Uzdin, and E. Poem, Experimental demonstration of quantum effects in the operation of microscopic heat engines, *Phys. Rev. Lett.* **122**, 110601 (2019).
- [20] J. Bengtsson, M. N. Tengstrand, A. Wacker, P. Samuelsson, M. Ueda, H. Linke, and S. M. Reimann, Quantum Szilard engine with attractively interacting bosons, *Phys. Rev. Lett.* **120**, 100601 (2018).
- [21] T. Fogarty and T. Busch, A many-body heat engine at criticality, *Quantum Sci. Technol.* **6**, 015003 (2021).
- [22] M. Boubakour, T. Fogarty, and T. Busch, Interaction-enhanced quantum heat engine, *Phys. Rev. Res.* **5**, 013088 (2023).
- [23] Y.-Y. Chen, G. Watanabe, Y.-C. Yu, X.-W. Guan, and A. del Campo, An interaction-driven many-particle quantum heat engine and its universal behavior, *npj Quantum Inf.* **5**, 88 (2019).
- [24] N. Yunger Halpern, C. D. White, S. Gopalakrishnan, and G. Refael, Quantum engine based on many-body localization, *Phys. Rev. B* **99**, 024203 (2019).
- [25] F. Carollo, F. M. Gambetta, K. Brandner, J. P. Garrahan, and I. Lesanovsky, Nonequilibrium quantum many-body Rydberg atom engine, *Phys. Rev. Lett.* **124**, 170602 (2020).
- [26] E. Geva and R. Kosloff, A quantum-mechanical heat engine operating in finite time. A model consisting of spin-1/2 systems as the working fluid, *J. Chem. Phys.* **96**, 3054 (1992).
- [27] D. von Lindenfels, O. Gräß, C. T. Schmiegelow, V. Kaushal, J. Schulz, M. T. Mitchison, J. Goold, F. Schmidt-Kaler, and U. G. Poschinger, Spin heat engine coupled to a harmonic-oscillator flywheel, *Phys. Rev. Lett.* **123**, 080602 (2019).
- [28] J. P. S. Peterson, T. B. Batalhão, M. Herrera, A. M. Souza, R. S. Sarthour, I. S. Oliveira, and R. M. Serra, Experimental characterization of a spin quantum heat engine, *Phys. Rev. Lett.* **123**, 240601 (2019).
- [29] W. Niedenzu and G. Kurizki, Cooperative many-body enhancement of quantum thermal machine power, *New J. Phys.* **20**, 113038 (2018).
- [30] M. Kloc, P. Cejnar, and G. Schaller, Collective performance of a finite-time quantum Otto cycle, *Phys. Rev. E* **100**, 042126 (2019).
- [31] K. Ono, S. N. Shevchenko, T. Mori, S. Moriyama, and F. Nori, Analog of a quantum heat engine using a single-spin qubit, *Phys. Rev. Lett.* **125**, 166802 (2020).
- [32] J. Wang, Z. Wu, and J. He, Quantum Otto engine of a two-level atom with single-mode fields, *Phys. Rev. E* **85**, 041148 (2012).
- [33] R. Wang, J. Wang, J. He, and Y. Ma, Efficiency at maximum power of a heat engine working with a two-level atomic system, *Phys. Rev. E* **87**, 042119 (2013).
- [34] T. D. Kieu, The second law, Maxwell's demon, and work derivable from quantum heat engines, *Phys. Rev. Lett.* **93**, 140403 (2004).
- [35] W. Ji, Z. Chai, M. Wang, Y. Guo, X. Rong, F. Shi, C. Ren, Y. Wang, and J. Du, Spin quantum heat engine quantified by quantum steering, *Phys. Rev. Lett.* **128**, 090602 (2022).
- [36] R. Kosloff and T. Feldmann, Discrete four-stroke quantum heat engine exploring the origin of friction, *Phys. Rev. E* **65**, 055102(R) (2002).
- [37] T. Feldmann and R. Kosloff, Quantum four-stroke heat engine: Thermodynamic observables in a model with intrinsic friction, *Phys. Rev. E* **68**, 016101 (2003).
- [38] T. Feldmann and R. Kosloff, Characteristics of the limit cycle of a reciprocating quantum heat engine, *Phys. Rev. E* **70**, 046110 (2004).
- [39] T. Zhang, W.-T. Liu, P.-X. Chen, and C.-Z. Li, Four-level entangled quantum heat engines, *Phys. Rev. A* **75**, 062102 (2007).
- [40] G. Zhang, Entangled quantum heat engines based on two two-spin systems with Dzyaloshinskii-Moriya anisotropic antisymmetric interaction, *Eur. Phys. J. D* **49**, 123 (2008).
- [41] H. Wang, S. Liu, and J. He, Thermal entanglement in two-atom cavity QED and the entangled quantum Otto engine, *Phys. Rev. E* **79**, 041113 (2009).

- [42] G. Thomas and R. S. Johal, Coupled quantum Otto cycle, *Phys. Rev. E* **83**, 031135 (2011).
- [43] F. Altintas, A. U. C. Hardal, and O. E. Müstecaplıoğlu, Quantum correlated heat engine with spin squeezing, *Phys. Rev. E* **90**, 032102 (2014).
- [44] F. Altintas and O. E. Müstecaplıoğlu, General formalism of local thermodynamics with an example: Quantum Otto engine with a spin-1/2 coupled to an arbitrary spin, *Phys. Rev. E* **92**, 022142 (2015).
- [45] V. Mehta and R. S. Johal, Quantum otto engine with exchange coupling in the presence of level degeneracy, *Phys. Rev. E* **96**, 032110 (2017).
- [46] S. Çakmak, F. Altintas, and Ö. E. Müstecaplıoğlu, Lipkin-Meshkov-Glick model in a quantum Otto cycle, *Europhys. J. Plus* **131**, 197 (2016).
- [47] L.-M. Zhao and G.-F. Zhang, Entangled quantum Otto heat engines based on two-spin systems with the Dzyaloshinski-Moriya interaction, *Quant. Inf. Process.* **16**, 216 (2017).
- [48] A. Hewgill, A. Ferraro, and G. De Chiara, Quantum correlations and thermodynamic performances of two-qubit engines with local and common baths, *Phys. Rev. A* **98**, 042102 (2018).
- [49] S. Chand and A. Biswas, Critical-point behavior of a measurement-based quantum heat engine, *Phys. Rev. E* **98**, 052147 (2018).
- [50] G. Piccitto, M. Campisi, and D. Rossini, The Ising critical quantum Otto engine, *New J. Phys.* **24**, 103023 (2022).
- [51] B. S. Revathy, V. Mukherjee, U. Divakaran, and A. del Campo, Universal finite-time thermodynamics of many-body quantum machines from Kibble-Zurek scaling, *Phys. Rev. Res.* **2**, 043247 (2020).
- [52] D. Porras and J. I. Cirac, Effective quantum spin systems with trapped ions, *Phys. Rev. Lett.* **92**, 207901 (2004).
- [53] J. W. Britton, B. C. Sawyer, A. C. Keith, C.-C. J. Wang, J. K. Freericks, H. Uys, M. J. Biercuk, and J. J. Bollinger, Engineered two-dimensional Ising interactions in a trapped-ion quantum simulator with hundreds of spins, *Nature (London)* **484**, 489 (2012).
- [54] J. G. Bohnet, B. C. Sawyer, J. W. Britton, M. L. Wall, A. M. Rey, M. Foss-Feig, and J. J. Bollinger, Quantum spin dynamics and entanglement generation with hundreds of trapped ions, *Science* **352**, 1297 (2016).
- [55] J. Zhang, G. Pagano, P. W. Hess, A. Kyprianidis, P. Becker, H. Kaplan, A. V. Gorshkov, Z.-X. Gong, and C. Monroe, Observation of a many-body dynamical phase transition with a 53-qubit quantum simulator, *Nature (London)* **551**, 601 (2017).
- [56] C. Monroe, W. C. Campbell, L.-M. Duan, Z.-X. Gong, A. V. Gorshkov, P. W. Hess, R. Islam, K. Kim, N. M. Linke, G. Pagano *et al.*, Programmable quantum simulations of spin systems with trapped ions, *Rev. Mod. Phys.* **93**, 025001 (2021).
- [57] F. Plastina, A. Alecce, T. J. G. Apollaro, G. Falcone, G. Francica, F. Galve, N. Lo Gullo, and R. Zambrini, Irreversible work and inner friction in quantum thermodynamic processes, *Phys. Rev. Lett.* **113**, 260601 (2014).
- [58] A. Dutta and J. K. Bhattacharjee, Phase transitions in the quantum Ising and rotor models with a long-range interaction, *Phys. Rev. B* **64**, 184106 (2001).
- [59] S. Fey and K. P. Schmidt, Critical behavior of quantum magnets with long-range interactions in the thermodynamic limit, *Phys. Rev. B* **94**, 075156 (2016).
- [60] N. Defenu, A. Trombettoni, and S. Ruffo, Criticality and phase diagram of quantum long-range  $O(N)$  models, *Phys. Rev. B* **96**, 104432 (2017).
- [61] L. Vanderstraeten, M. Van Damme, H. P. Büchler, and F. Verstraete, Quasiparticles in quantum spin chains with long-range interactions, *Phys. Rev. Lett.* **121**, 090603 (2018).
- [62] Z. Zhu, G. Sun, W.-L. You, and D.-N. Shi, Fidelity and criticality of a quantum Ising chain with long-range interactions, *Phys. Rev. A* **98**, 023607 (2018).
- [63] E. Gonzalez Lazo, M. Heyl, M. Dalmonte, and A. Angelone, Finite-temperature critical behavior of long-range quantum Ising models, *SciPost Phys.* **11**, 076 (2021).
- [64] J. A. Koziol, A. Langheld, S. C. Kapfer, and K. P. Schmidt, Quantum-critical properties of the long-range transverse-field Ising model from quantum Monte Carlo simulations, *Phys. Rev. B* **103**, 245135 (2021).
- [65] M. Born and V. Fock, Beweis des adiabatsatzes, *Z. Angew. Phys.* **51**, 165 (1928).
- [66] T. Kato, On the adiabatic theorem of quantum mechanics, *J. Phys. Soc. Jpn.* **5**, 435 (1950).
- [67] J. E. Avron and A. Elgart, Adiabatic theorem without a gap condition, *Commun. Math. Phys.* **203**, 445 (1999).
- [68] D. J. Griffiths and D. F. Schroeter, *Introduction to Quantum Mechanics*, 3rd ed. (Cambridge University Press, Cambridge, 2018).
- [69] T. Holstein and H. Primakoff, Field dependence of the intrinsic domain magnetization of a ferromagnet, *Phys. Rev.* **58**, 1098 (1940).
- [70] A. Peres, Separability criterion for density matrices, *Phys. Rev. Lett.* **77**, 1413 (1996).
- [71] M. Horodecki, P. Horodecki, and R. Horodecki, Separability of mixed states: Necessary and sufficient conditions, *Phys. Lett. A* **223**, 1 (1996).
- [72] G. Tóth and O. Gühne, Entanglement and permutational symmetry, *Phys. Rev. Lett.* **102**, 170503 (2009).
- [73] P. Pfeuty, The one-dimensional Ising model with a transverse field, *Ann. Phys.* **57**, 79 (1970).
- [74] A. E. Allahverdyan, R. S. Johal, and G. Mahler, Work extremum principle: Structure and function of quantum heat engines, *Phys. Rev. E* **77**, 041118 (2008).
- [75] A. Campa, T. Dauxois, and S. Ruffo, Statistical mechanics and dynamics of solvable models with long-range interactions, *Phys. Rep.* **480**, 57 (2009).
- [76] N. Defenu, T. Donner, T. Macrì, G. Pagano, S. Ruffo, and A. Trombettoni, Long-range interacting quantum systems, *Rev. Mod. Phys.* **95**, 035002 (2023).
- [77] M. Kac, G. E. Uhlenbeck, and P. C. Hemmer, On the van der Waals theory of the vapor-liquid equilibrium. I. Discussion of a one-dimensional model, *J. Math. Phys.* **4**, 216 (1963).
- [78] M. Kac and C. J. Thompson, Critical behavior of several lattice models with long-range interaction, *J. Math. Phys.* **10**, 1373 (1969).
- [79] S. A. Cannas and F. A. Tamarit, Long-range interactions and nonextensivity in ferromagnetic spin models, *Phys. Rev. B* **54**, R12661 (1996).
- [80] G. Thomas, M. Banik, and S. Ghosh, Implications of coupling in quantum thermodynamic machines, *Entropy* **19**, 442 (2017).

- [81] M. Demirplak and S. A. Rice, Adiabatic population transfer with control fields, *J. Phys. Chem. A* **107**, 9937 (2003).
- [82] M. V. Berry, Transitionless quantum driving, *J. Phys. A: Math. Theor.* **42**, 365303 (2009).
- [83] A. del Campo, M. M. Rams, and W. H. Zurek, Assisted finite-rate adiabatic passage across a quantum critical point: Exact solution for the quantum Ising model, *Phys. Rev. Lett.* **109**, 115703 (2012).
- [84] A. del Campo, Shortcuts to adiabaticity by counterdiabatic driving, *Phys. Rev. Lett.* **111**, 100502 (2013).
- [85] S. Deffner, C. Jarzynski, and A. del Campo, Classical and quantum shortcuts to adiabaticity for scale-invariant driving, *Phys. Rev. X* **4**, 021013 (2014).
- [86] H. Saberi, T. Opatrny, K. Mølmer, and A. del Campo, Adiabatic tracking of quantum many-body dynamics, *Phys. Rev. A* **90**, 060301(R) (2014).
- [87] S. Campbell, G. De Chiara, M. Paternostro, G. M. Palma, and R. Fazio, Shortcut to adiabaticity in the Lipkin-Meshkov-Glick model, *Phys. Rev. Lett.* **114**, 177206 (2015).
- [88] G. Passarelli, V. Cataudella, R. Fazio, and P. Lucignano, Counterdiabatic driving in the quantum annealing of the  $p$ -spin model: A variational approach, *Phys. Rev. Res.* **2**, 013283 (2020).
- [89] I. Čepaitė, A. Polkovnikov, A. J. Daley, and C. W. Duncan, Counterdiabatic optimized local driving, *PRX Quantum* **4**, 010312 (2023).
- [90] D. Sels and A. Polkovnikov, Minimizing irreversible losses in quantum systems by local counterdiabatic driving, *Proc. Natl. Acad. Sci. USA* **114**, E3909 (2017).
- [91] M. Kolodrubetz, D. Sels, P. Mehta, and A. Polkovnikov, Geometry and non-adiabatic response in quantum and classical systems, *Phys. Rep.* **697**, 1 (2017).
- [92] A. Hartmann, V. Mukherjee, W. Niedenzu, and W. Lechner, Many-body quantum heat engines with shortcuts to adiabaticity, *Phys. Rev. Res.* **2**, 023145 (2020).
- [93] F. L. Curzon and B. Ahlborn, Efficiency of a Carnot engine at maximum power output, *Am. J. Phys.* **43**, 22 (1975).
- [94] T. Feldmann and R. Kosloff, Quantum lubrication: Suppression of friction in a first-principles four-stroke heat engine, *Phys. Rev. E* **73**, 025107(R) (2006).
- [95] Q. Wang, Performance of quantum heat engines under the influence of long-range interactions, *Phys. Rev. E* **102**, 012138 (2020).
- [96] A. Solfanelli, G. Giachetti, M. Campisi, S. Ruffo, and N. Defenu, Quantum heat engine with long-range advantages, *New J. Phys.* **25**, 033030 (2023).
- [97] P. Sgroi, G. M. Palma, and M. Paternostro, Reinforcement learning approach to nonequilibrium quantum thermodynamics, *Phys. Rev. Lett.* **126**, 020601 (2021).
- [98] A. Rolandi, M. Perarnau-Llobet, and H. J. Miller, Optimal control of dissipation and work fluctuations for rapidly driven systems, *New J. Phys.* **25**, 073005 (2023).
- [99] S. Deffner and M. V. S. Bonança, Thermodynamic control—An old paradigm with new applications, *Europhys. Lett.* **131**, 20001 (2020).
- [100] V. Cavina, P. A. Erdman, P. Abiuso, L. Tolomeo, and V. Giovannetti, Maximum-power heat engines and refrigerators in the fast-driving regime, *Phys. Rev. A* **104**, 032226 (2021).
- [101] A. Soriani, E. Miranda, S. Deffner, and M. V. S. Bonança, Shortcuts to thermodynamic quasistaticity, *Phys. Rev. Lett.* **129**, 170602 (2022).
- [102] P. A. Erdman, A. Rolandi, P. Abiuso, M. Perarnau-Llobet, and F. Noé, Pareto-optimal cycles for power, efficiency and fluctuations of quantum heat engines using reinforcement learning, *Phys. Rev. Res.* **5**, L022017 (2023).
- [103] G. Facchinetti, S. D. Jenkins, and J. Ruostekoski, Storing light with subradiant correlations in arrays of atoms, *Phys. Rev. Lett.* **117**, 243601 (2016).
- [104] G. Facchinetti and J. Ruostekoski, Interaction of light with planar lattices of atoms: Reflection, transmission, and cooperative magnetometry, *Phys. Rev. A* **97**, 023833 (2018).
- [105] L. A. Williamson and J. Ruostekoski, Optical response of atom chains beyond the limit of low light intensity: The validity of the linear classical oscillator model, *Phys. Rev. Res.* **2**, 023273 (2020).
- [106] L. A. Williamson, M. O. Borgh, and J. Ruostekoski, Superatom picture of collective nonclassical light emission and dipole blockade in atom arrays, *Phys. Rev. Lett.* **125**, 073602 (2020).
- [107] A. Cidrim, T. S. do Espirito Santo, J. Schachenmayer, R. Kaiser, and R. Bachelard, Photon blockade with ground-state neutral atoms, *Phys. Rev. Lett.* **125**, 073601 (2020).
- [108] D. Gunlycke, V. M. Kendon, V. Vedral, and S. Bose, Thermal concurrence mixing in a one-dimensional Ising model, *Phys. Rev. A* **64**, 042302 (2001).
- [109] T. J. Osborne and M. A. Nielsen, Entanglement in a simple quantum phase transition, *Phys. Rev. A* **66**, 032110 (2002).
- [110] B. V. Fine, F. Mintert, and A. Buchleitner, Equilibrium entanglement vanishes at finite temperature, *Phys. Rev. B* **71**, 153105 (2005).
- [111] T. Yu and J. H. Eberly, Sudden death of entanglement, *Science* **323**, 598 (2009).
- [112] M. Vogl, P. Laurell, H. Zhang, S. Okamoto, and G. A. Fiete, Resummation of the Holstein-Primakoff expansion and differential equation approach to operator square roots, *Phys. Rev. Res.* **2**, 043243 (2020).
- [113] J. König and A. Hucht, Newton series expansion of bosonic operator functions, *SciPost Phys.* **10**, 007 (2021).
- [114] L. Cevolani, G. Carleo, and L. Sanchez-Palencia, Spreading of correlations in exactly solvable quantum models with long-range interactions in arbitrary dimensions, *New J. Phys.* **18**, 093002 (2016).
- [115] J. Wu, X. Zhang, and D. Liu, An efficient calculation of the Clausen functions  $Cl_n(\theta)$  ( $n \geq 2$ ), *Bit Numer. Math.* **50**, 193 (2010).